Metal-Induced Crystallization in Metal Oxides

Laurent Lermusiaux, Antoine Mazel, Adrian Carretero-Genevrier, Clément Sanchez, Glenna L. Drisko

ACCOUNTS of chemical research

pubs.acs.org/accounts

Article

Metal-Induced Crystallization in Metal Oxides

Laurent Lermusiaux, Antoine Mazel, Adrian Carretero-Genevrier, Clément Sanchez,* and Glenna L. Drisko*

Cite This: https://doi.org/10.1021/acs.accounts.1c00592

Read Online

ACCESS | Metrics & More | Article Recommendations

CONSPECTUS: The properties of a material depend upon its physical characteristics, one of these being its crystalline state. Next generation solid-state technologies will integrate crystalline oxides into thermal sensitive processes and composite materials. Crystallization of amorphous phases of metal oxides in the solid state typically requires substantial energy input to induce the amorphous to crystalline phase transformation. In the case of silica, the transformation to α-quartz in a furnace occurs above 1300 °C and that of titania, above 400 °C. These calcination processes are costly in energy but also often degrade complex material architectures or compositions.

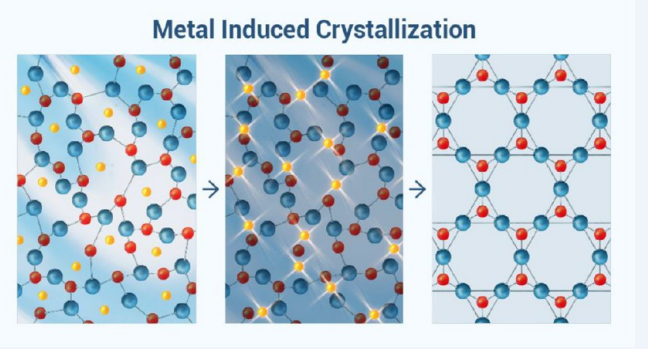

Thus, low temperature crystallization techniques are required that preserve macro- and mesostructures and complex elemental composition (e.g., organic-, metal-, and semiconductor-metal oxide hybrids/composites). Some solution-based techniques exist to directly fabricate crystalline metal oxides. However, these are not always compatible with the specificities of the system or industrial constraints. A postsynthetic, solid-state approach that reduces crystallization temperature in metal oxides is metal-induced crystallization (MIC).

MIC is the introduction of catalytic amounts of a cation, which can be an s-block, p-block, or d-block cation, that migrates through the solid metal oxide lattice. The cation is thought to temporarily break metal oxide bonds, allowing [MO_x] polyhedra to rotate and reform bonds with neighboring [MO_x] groups in a lower energy crystalline phase. Depending on the system, the cation can favor or defavor the formation of a particular crystalline phase, providing a means to tune the purity and crystalline phase ratios. An advantage of MIC is that, although the crystallization occurs in the solid state, the crystallization process can be accomplished for particle suspensions in liquid media. In this case, the energy required to induce the crystallization can come from, for example, a microwave or an ultrasound bath. The crystallization of particles in suspension avoids aggregation from particle−particle sintering. In the case of thin films, the energy for crystallization typically comes from a laser or calcination.

MIC is only recently being used as a low temperature metal oxide crystallization technique, despite being widely used in the semiconductor industry. Here, the mechanism and previous studies in MIC are presented for titania, silica, and other oxides. The beauty of this technique is that it is extremely easy to employ: cations can be incorporated into the system postsynthetically and then are often expelled from the lattice upon phase conversion. We expect MIC to enrich materials for photochromic, optoelectronic, catalyst, biological, and other applications.

KEY REFERENCES

- Danty, P. M. P.; Mazel, A.; Cormary, B.; De Marco, M. L.; Allouche, J.; Flahaut, D.; Jimenez-Lamana, J.; Lacomme, S.; Delville, M.-H.; Drisko, G. L. Microwave-Assisted and Metal-Induced Crystallization: A Rapid and Low Temperature Combination. *Inorg. Chem.* **2020**, *59* (9), 6232−6241.[1] The structure is preserved in titania spheres, crystallized at 150 °C in suspension. This article opens the door toward hybrid materials with postsynthetically crystallized TiO_2.
- Drisko, G. L.; Carretero-Genevrier, A.; Perrot, A.; Gich, M.; Gàzquez, J.; Rodriguez-Carvajal, J.; Favre, L.; Grosso, D.; Boissière, C.; Sanchez, C. Crystallization of Hollow Mesoporous Silica Nanoparticles. *Chem. Commun.* **2015**, *51* (20), 4164−4167.[2] The relationship between the cationic devitrification agent and the obtained crystal phase is studied in the MIC of SiO_2. Macrostructured hollow spheres preserve their form

Received: September 23, 2021

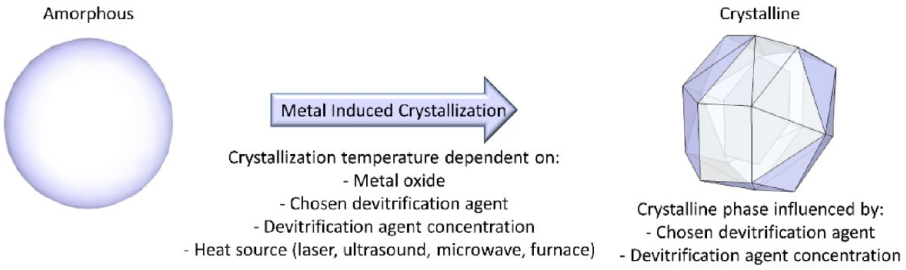

Figure 1. Presence of devitrification agents in an amorphous oxide lowers the crystallization temperature but also impacts the crystalline phase, allowing phase ratios to be finely tuned.

Table 1. Metal-Induced Crystallization Conditions for Amorphous Titania

devitrification agent	onset temperature (°C)	phase	comments	reference
$Co(NO_3)_2$	223	anatase, rutile	powder containing 2 mol % Co relative to TiO_2, 514.5 nm laser used, energy density of 15 W/mm^2	17
$HAuCl_4$	80	anatase	sonochemical treatment of a powder combined with MIC	19
$AgNO_3$	190	anatase, rutile	thermal treatment of nanoparticles, phase transition temperature dependent on the atmosphere (air vs N_2)	32
$AgNO_3$	250	anatase, rutile	thermal annealing of thin films	33
$AgNO_3$	250	anatase, rutile	thermal annealing of nanoparticles	34
Cu	210	anatase	thermal annealing of thin films, postsynthetic diffusion	26
Ni	220	anatase	thermal annealing of thin films, postsynthetic diffusion	25
Au	250	anatase	thermal annealing of thin films, postsynthetic diffusion	27
Ni, Au, or Pt	350	anatase	thermal annealing of thin films, postsynthetic diffusion	35
$Zn(NO_3)_2$, $NaNO_3$, $Co(NO_3)_2$, $La(NO_3)_3$, $Al(NO_3)_3$, $Ca(NO_3)_2$, KNO_3, and $BaNO_3$	350	anatase, rutile	thermal annealing of powders	36
KCl, $CoCl_2$, $NiCl_2$, $CuCl_2$, $ZnCl_2$, $MnCl_2$, and $AlCl_3$	150	anatase	microwave irradiation of titania microspheres	1

during this crystallization process, leading to hard, low density α-quartz structures.

- Carretero-Genevrier, A.; Gich, M.; Picas, L.; Gazquez, J.; Drisko, G. L.; Boissiere, C.; Grosso, D.; Rodriguez-Carvajal, J.; Sanchez, C. Soft-Chemistry-Based Routes to Epitaxial α-Quartz Thin Films with Tunable Textures. *Science* **2013**, *340* (6134), 827−831.[3] We show MIC for the first time in silica films crystallized on a silicon substrate. The epitaxial relationship between the substrate and the gel dictates the direction of α-quartz crystal growth. Mesostructures are preserved during the epitaxial growth.
- Drisko, G. L.; Carretero-Genevrier, A.; Gich, M.; Gàzquez, J.; Ferrah, D.; Grosso, D.; Boissière, C.; Rodriguez-Carvajal, J.; Sanchez, C. Water-Induced Phase Separation Forming Macrostructured Epitaxial Quartz Films on Silicon. *Adv. Funct. Mater.* **2014**, *24* (35), 5494−5502.[4] Macroperforated, mono-oriented α-quartz films are produced. The importance of the cation concentration within the gel on the MIC process is explored and demonstrated.

1. INTRODUCTION

The physical properties of a material are highly dependent on its crystalline phase, and many crystalline materials have significantly different properties from their amorphous counterpart and other crystal allotropes. The classic example is that of carbon, which can exist as charcoal (amorphous state), diamond (face centered cubic structure), or graphite (either hexagonal or rhombohedral structure), each allotrope exhibiting vastly different physical properties. In the example of silicon particles, the intensity and the frequency of their optical resonances are highly influenced by the crystalline state.[10] Turning to a metal oxide, the photocatalytic activity[11] and the toxicity[12] of titania are both highly dependent on crystalline phase. Piezoelectricity is well-known in α-quartz but absent in amorphous silica.

Crystallization is most often achieved via calcination, where a sample is heated to high temperatures to initiate the amorphous to crystalline transition. Calcination can pose several problems; principally, it can lead to particle−particle sintering and is highly energy consuming. In the case of SiO_2, the oxide typically remains amorphous until at least 1300 °C,[13] making it hard to preserve mesostructured materials upon crystallization. One way to decrease crystallization temperature, conserve energy, retain the mesostructure, and ensure crystalline phase purity or produce hybrid crystalline materials is to use a technique called metal-induced crystallization (MIC) (Figure 1). MIC is a fully solid-state process, whereupon one material crystallizes at a lower temperature via contact with a metal that does not form part of the lattice.[7]

The first report of MIC was in 1970 with the crystallization of amorphous germanium by noble metals, aluminum, and tin.[14] Soon after, amorphous silicon was also devitrified at a lowered temperature by metals.[15] The terminology "metal-induced crystallization" is not used often with regard to silica crystallization, but the concept of devitrification using lattice modifiers has been known since the early 1900s.[8,9] The effect of dopants on titania crystallization via laser irradiation was first noticed in 1996.[17] Ten years later, the first MIC of titania

https://doi.org/10.1021/acs.accounts.1c00592
Acc. Chem. Res. XXXX, XXX, XXX−XXX

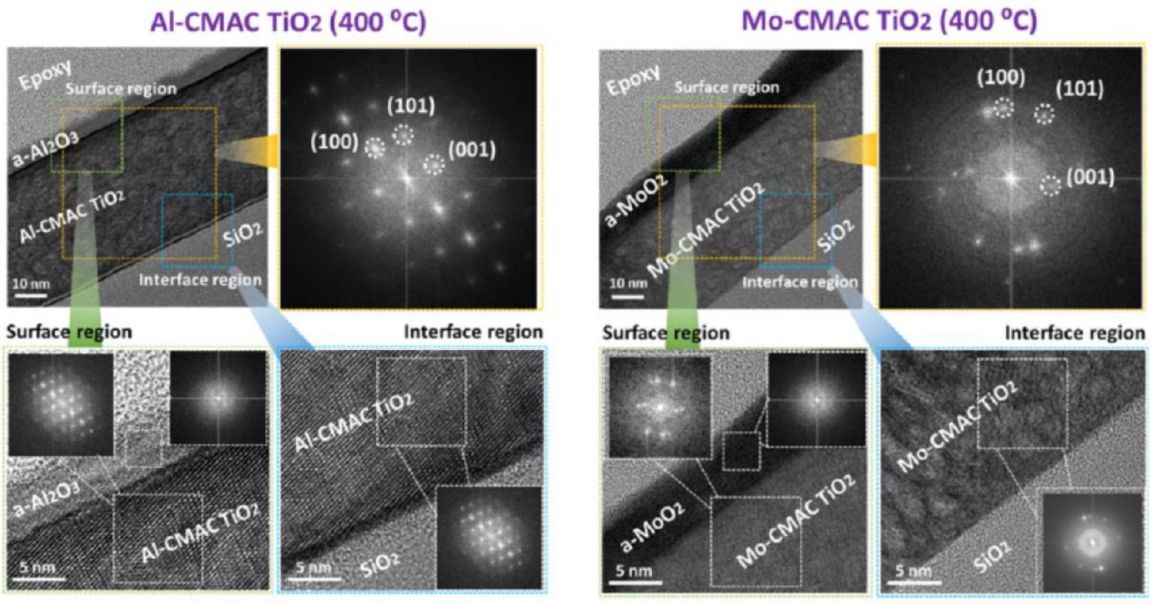

Figure 2. High resolution electron microscopy images of thin films with a top coat of either aluminum (left) or molybdenum (right) with diffraction patterns showing their overall degree of crystallinity and local crystallinity at both the metal oxide/TiO_2 interface and the TiO_2/glass substrate interface. Adapted from ref 37. Copyright 2020 American Chemical Society.

during classical calcination via metal contamination was reported.[18,19] However, despite the past 25 years of research into the MIC of oxides, this Account is the first overview on this topic. Here, we present the advances in titania, silica, and other metal oxides crystallized using MIC.

2. TITANIA

2.1. Crystalline Phase Control

Crystalline titania appears in a wide variety of applications, as photocatalysts and photovoltaics, and in a number of food and agricultural products, its crystalline phase is one of the factors impacting its properties. There are three common phases in titania: anatase, brookite, and rutile with anatase and rutile being the most commonly obtainable forms and anatase requiring the least energy to be achieved. Not only do metal cations impact the amorphous to anatase transition, but also they can promote or retard the transformation to either brookite or rutile. In these sections, we will briefly discuss the impact of metal cations on crystalline phase transition; see refs 20−24 for a deeper discussion of this topic. A summary of titania materials produced to date via MIC is presented in Table 1.

2.2. Mechanism of Metal-Induced Crystallization in Titania

Several studies on the mechanism of MIC reported that the metal diffuses throughout the titania structure, whether or not it was originally in the gel.[24−28] The cations, typically acting as crystallization catalysts, do not systematically dope the final oxide. Yang et al. proposed that the metals help to rearrange the Ti−O bonds into an energetically more favorable crystalline arrangement.[25] The Ti−O bond weakens when a metal cation partially transfers valence electrons to the antibonding orbitals of the Ti−O bond. Heat, coming from an external source, breaks the weakened Ti−O bonds as well as the metal−oxygen bond. Crystalline TiO_2, having free energy lower than that of its amorphous counterpart,[29] results in the cation remaining mobile in the gel. By studying the effect of cation dopants on the phase transition of anatase to rutile,[29] Nair et al. proposed that cations having a radius comparable to Ti^{4+} (60.5 pm) and a charge of less than +4 can occupy a lattice point and thus increase the oxygen vacancy concentration. However, larger cations find themselves in interstitial positions and thus decrease oxygen vacancies. They correlated increased oxygen vacancy concentration with a lower onset of crystal nucleation,[29] which is complementary to the mechanism proposed by Yang et al.[25] Electron paramagnetic resonance studies of the local metals' environment within titania gels and crystals have indicated that the cation does not diffuse alone but with some of its ligands.[30]

2.3. Crystallization Coupling Metal-Induced Crystallization to Different Annealing Techniques

2.3.1. Laser Annealing. Raman lasers can be used to anneal doped and nondoped titania samples to produce thin films containing crystalline anatase and/or rutile phases.[17] Camacho-López et al. demonstrated that the required power density to induce phase transformation is 20 times lower in the presence of 2 mol % Co^{2+} than without the metal additive.[31] Moreover, the quantity of crystalline material increased with time, and the type of crystalline phase depended on the quantity of cobalt in the titania film.[31]

2.3.2. Ultrasound Treatment. Sonochemistry, combined with MIC, was first reported as a means to crystallize titania in 2006.[19] For example, in ethylene glycol, sonicating amorphous titania led to its crystallization when in the presence of $HAuCl_4$.

2.3.3. Convective Heating. Convective heating has been combined with the MIC of titania in two main ways, via incorporation of a cation prior to the sol−gel transition and by postsynthetic diffusion of a metal from a metallic contact layer. Both methods have similar crystallization temperatures.

Rodríguez-Talavera et al. observed the MIC of titania using La, Zn Al, K, Na, Ca, Ba, and Co.[36] The onset crystallization temperature did not depend on the nature of the cation employed, but there was a good correlation between the

https://doi.org/10.1021/acs.accounts.1c00592
Acc. Chem. Res. XXXX, XXX, XXX−XXX

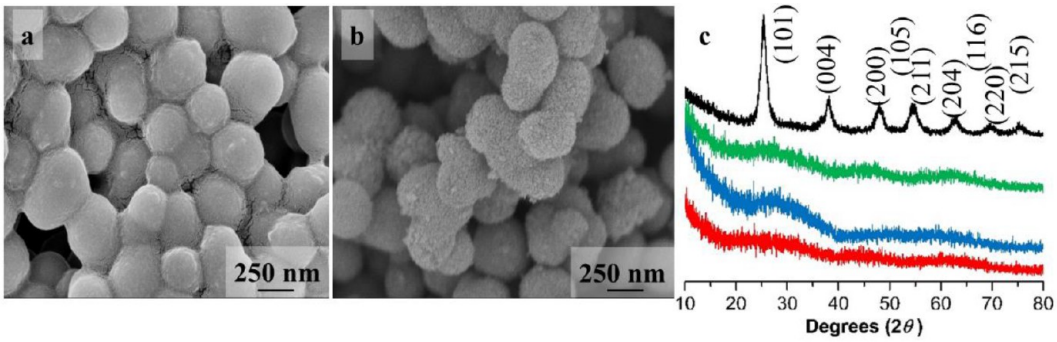

Figure 3. SEM images of amorphous titania (a) before and (b) after MIC under microwave irradiation. (c) X-ray diffractograms of titania before treatment (red), after calcination of Mn^{2+} doped titania at 150 °C (blue), after microwave treatment of TiO_2 at 150 °C (green), and after of Mn^{2+}-containing titania at 150 °C (black). Reproduced from ref 1. Copyright 2020 American Chemical Society.

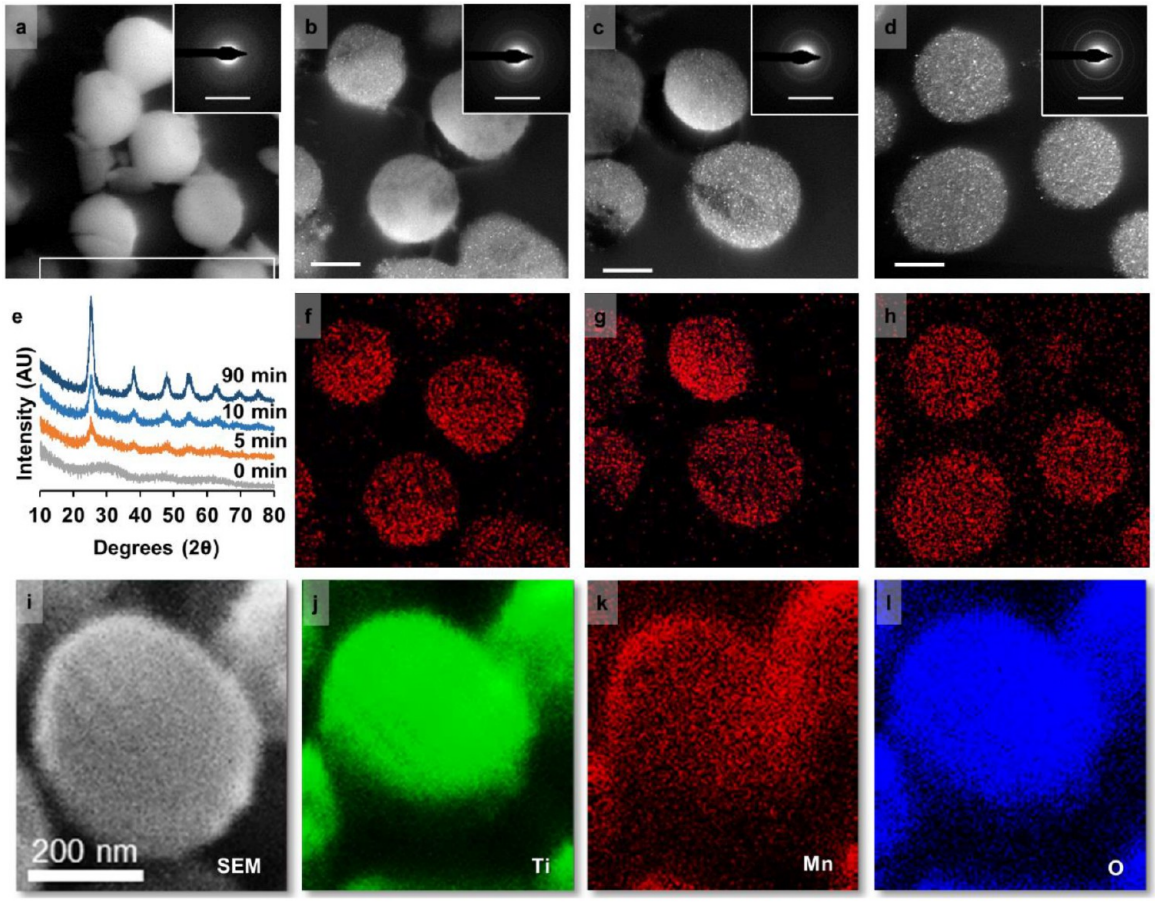

Figure 4. Bright field TEM images of ultramicrotomed sections of beads (a) prior to contact and after (b) 5, (c) 10, and (d) 90 min of exposure to the cation and microwaves. The scale bars represent 1 μm. The inset represents the SAED pattern of a large collection of particles from each sample. (e) The XRD diffraction pattern, ranging from no treatment (gray) to 90 min of irradiation time (dark blue). (f–h) The EDX analysis for Mn (red) for the corresponding micrographs of (b–d). (i) SEM image and scanning Auger mapping of a single particle treated with microwaves for 10 min containing (j) titanium, (k) manganese, and (l) oxygen. Adapted from ref 1. Copyright 2020 American Chemical Society.

temperature of the phase transition from anatase to rutile. The authors attributed the stabilization of the anatase phase to the cation size and oxidation state.

García-Serrano et al. studied the addition of $AgNO_3$ to the precursor mixture before the sol–gel reaction and found that crystallite size decreased with increasing $AgNO_3$ concentration.[32] Small crystallite size is commonly observed in MIC because, according to Amarjargal et al., the cation lowers the crystallization temperature, leading to widespread nucleation and a high density of grain boundaries.[34] However, the cation is then typically ejected from the lattice, as its size is incompatible with insertion/substitution. As the cation moves to the crystallite surface, the impetus for grain boundary migration decreases.

The MIC of titania is achievable by conductive heating of TiO_2 in contact with a metallic layer. The mechanism of crystallization of thin films using a gold layer was studied via Raman imaging and showed that very small and sparse

https://doi.org/10.1021/acs.accounts.1c00592
Acc. Chem. Res. XXXX, XXX, XXX–XXX

Table 2. Metal-Induced Crystallization Conditions for Amorphous Silica

devitrification agent	onset temperature (°C)	phase	comments	reference
$CaCO_3$	975	α-quartz	peak intensity increases with calcination temperature	41
$CaCO_3$	1100	α-cristobalite		41
$AgNO_3$	500	cristobalite		16
$HAuCl_4$	950	β-cristobalite		19
Au^{3+} or Na^+	900	cristobalite	2.2 wt % Au with 0.6−1.3% Na contained in the SiO_2	42
$CaCl_2$, $Sr(NO_3)_2$, or $BaCl_2$	800	α-quartz	0.01−0.03 mol % devitrification agent/Si	3, 4
$MgCl_2$, $CaCl_2$, $SrCl_2$, and $BaCl_2$		α-quartz	0.1 mol % Mg^{2+}, 0.025 mol % Ca^{2+}, 0.02 mol % Sr^{2+}, and 0.01 mol % Ba^{2+} in SiO_2	2
$LiNO_3$	870	α-quartz	infiltrated with a 0.5 M solution	43
$MgCl_2$	1100	α-quartz	0.1 mol % Mg^{2+}	44
$SrCl_2$	1000	α-quartz	0.03−0.10 ratio of Sr/SiO_2	45
Na_2O flux	750	cristobalite	SiO_2 spheres contained in a carbon matrix containing the flux	6

crystallites appear at 250 °C.[27] The density of crystallites increases with annealing temperature; it seems that the crystallites do not grow in size, but rather, more small crystallites nucleate within the film. Yang et al.[27] found that, when TiO_2 was deposited on a thin contact film, Ni and Cu participated in the MIC to a higher degree than Au and NiO contact films. Cu or Ni migrates from a bottom layer to the top layer of TiO_2, producing fully crystalline anatase. The difference in the metals was attributed to their difference in electronegativity, which is inversely proportional to their ability to transfer electrons from the metal to the antibonding orbitals of the Ti−O bond. Similarly, metallic layers can be deposited above amorphous titania to create crystalline thin film transistors.[37] Shin et al.[37] showed that Al-, Mo-, and Ti-induced crystallization at relatively low temperatures, but Al produced larger grain sizes, a higher degree of crystallization, and enhanced electron transport (Figure 2). In the Ti and Mo films, crystallization occurred close to the metal oxide/titania interface. The films produced via Al-induced crystallization displayed enhanced electrical transport performance in the semiconductor film.

2.3.4. Microwave Irradiation. We were the first to combine MIC and microwave heating, where using both techniques in concert lowers the temperature of titania crystallization (Figure 3).[1] The heat treatment temperature reduced from a minimum of 400 °C in a classical convective heating process to 150 °C in the microwave. Treatment time is similarly reduced from several hours in a furnace to 10 min (including heating and cooling times). An advantage of this combinatorial approach is that titania nanomaterials can be crystallized in water, avoiding particle−particle sintering and maintaining the particles in solution, which can readily be processed into a material.

We tested the ability of Mn^{2+}, Co^{2+}, Ni^{2+}, Al^{3+}, Cu^{2+}, and Zn^{2+} to devitrify titania in the microwave reactor.[1] All of these cations created anatase at 150 °C in the microwave with the crystallite size being dependent on the ionic radius of the cation. The migration of the cation throughout the TiO_2 lattice occurred prior to crystallization (Figure 4). Oddly, we noticed that titania microspheres seemed either amorphous or well crystalline (Figure 4b,c), but partially crystallized microspheres were rarely observed. As the crystalline grains are small in all cases, it is hard to understand why the onset of nucleation occurs at different times in different microspheres, but once initiated, the amorphous material quickly converts to a polycrystalline sample.

2.4. Applications

One of the major advantages of the MIC of titania is the ability to get relatively pure phases of rutile at relatively low temperature,[24] which show better wettability and increased optical absorption in the red, needed for photocatalytic antimicrobial coatings. Many electronic and optoelectronic devices are fabricated on substrates that are thermally unstable.[27] Titania can be used in resistive switching for use in memory devices; however, its crystalline form must be obtained, preferably on a glass substrate. These metal-containing titania films produced photoluminescent films with tailorable switching properties.[24]

Further research efforts should also examine the role of the metal's chemical nature, concentration, and oxidation state. For instance, it was observed that $AuCl_3$ and clusters of Au_{11}^{3+} incorporated into TiO_2 influenced both phase purity and catalytic activity.[38] The reasons why different phases are observed when a different devitrification agent is observed remain obscure.

3. SILICA

3.1. Crystalline Phase Control

There are three common polymorphs of crystalline SiO_2: α-quartz, cristobalite, and tridymite, where α-quartz is the most stable.[16] MIC commonly yields either α-quartz or cristobalite with many aspects impacting the MIC of silica, including the morphology of the vitreous material, the type and quantity of cation used, and the presence of a crystalline interface with the silica gel (leading to epitaxial crystal growth). SiO_2 materials produced using MIC are presented in Table 2. Silicates can also occur for certain cations, particularly if cation concentration in the SiO_2 lattice is too high.[2] Just as in classical crystallization techniques, the degree of crystallinity will increase by increasing the time and temperature of the crystallization.[19] The obtained crystalline phase and the ratio of quartz to cristobalite are also dependent on the calcination time and temperature.

MIC in silica is thought to occur via the reorganization of $[SiO_4]$ tetrahedra, as is the case for TiO_2. In both the amorphous and crystalline states, the oxygen atoms forming the vertices are shared by two adjacent tetrahedra.[39] Network modifiers, which are typically mobile cation species, break the connections between these $[SiO_4]$ tetrahedra, allowing them to freely move to reorganize into a lower energy, crystalline phase.[39,40]

https://doi.org/10.1021/acs.accounts.1c00592
Acc. Chem. Res. XXXX, XXX, XXX−XXX

3.2. Impact of Amorphous Silica Morphology on Crystallization

The morphology of silica can impact the capacity of MIC in two ways. The first is the distribution of devitrification agents throughout the material; the second is related to the ability of the SiO_2 to shrink as it crystallizes. Although the ions move through solid-state silica, mesoporosity allows a homogeneous distribution of these ions throughout the material before heat treatment begins. Mesoporosity additionally accommodates volume changes, permitting the lattice to shrink during crystallization.

Garnica-Romo et al. studied the impact of the amorphous silica structure on crystallization by changing the H_2O/TEOS molar ratio during synthesis.[16] The authors obtained highly crystalline cristobalite after heat treatment at 800 °C at the relatively low H_2O/TEOS molar ratio of 3.5. However, as the quantity of water in the sol−gel solution increased, the quality of the crystallization diminished.

To study the influence of porosity on the crystallization behavior, mesoporous (SBA-15) and nonporous SiO_2 (Cab-O-Sil) were functionalized with gold nanoparticles and treated at 900 °C.[42] SBA-15 crystallized to cristobalite, while Cab-O-Sil remained amorphous. The authors believe that the difference is due to the sample's structure.[42] SBA-15 has thin walls and a large pore volume that would better accommodate local volume changes upon crystallization. Cab-O-Sil has large grains, which are more likely to preserve the structure of the amorphous material.

Okabayashi et al. attempted the crystallization of spherical particles with three different spatial distributions of calcium (Figure 5).[41] When heated to 1000 °C for an hour, only the particles with Ca placed in the core did not crystallize. The authors concluded that crystallization must begin at the particle surface.

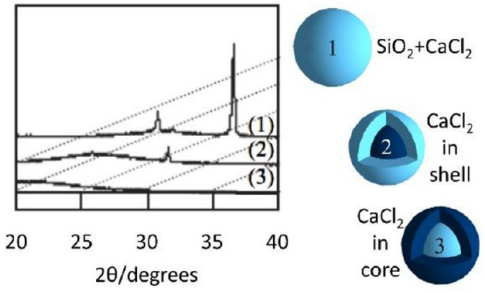

Figure 5. Diffractograms of spherical particles containing the devitrification agent partitioned throughout, solely in the shell or solely in the core. Adapted with permission from ref 41. Copyright 2005 The Chemical Society of Japan.

3.3. Nature and Quantity of the Devitrification Agent

We previously showed that, among many different cations, only Sr^{2+}, Ba^{2+}, and Ca^{2+} demonstrated epitaxial growth of macroporous α-quartz films on (100) silicon substrates.[4] To understand the mechanism, the ratio of Sr^{2+} to SiO_2 was varied and correlated to the quality and orientation of α-quartz films (Figure 6a,b).[45] For ratios larger than 0.05, the microstructure is dominated by α-quartz densification that significantly decreases the mosaicity of the films (Figure 6c).

In our work in thin films, we reported testing Li^+, Na^+, Sr^{2+}, Mn^{2+}, Fe^{2+} /Fe^{3+}, Ca^{2+}, Ce^{3+}, and La^{3+}, where only some of these led to SiO^2 crystallization.[4] Of the series of cations that did not induce silica crystallization,[4] it is likely that at least some of these are able to crystallize silica but that the conditions were not suitable. We showed that, in the crystallization of hollow silica particles using alkaline earth metals, the minimum salt concentration needed to induce crystallization decreases as the cation radius increases (Figure 7).[2] When the concentration was suboptimal, residual amorphous silica was present. Higher quantities of devitrification agent are needed for smaller cations than for larger ions, as the ratio of nonbridging oxygens/Si in glass increases as a function of cation size.[46] Venezia et al. found differing results: for larger atoms, namely, potassium and cesium, crystallization only occurred with high concentrations of alkali ions.[5] Moreover, the concentration of sodium impacted the transition temperature of silica to cristobalite: the higher the concentration of devitrification agent, the lower was the temperature of the transition.

Matsuno et al. infiltrated a colloidal crystal of silica with Li^+ and, then, encased the silica spheres in a matrix of poly(furfuryl alcohol).[43] Li^+ melted the silica completely, followed by crystallization within a carbon scaffold, producing a monocrystalline quartz superlattice with grains several micrometers in size (Figure 8). This same group has recently adapted their synthesis method using $NaNO_2$ dissolved into a phenolic resin to serve as the carbon scaffold to achieve mesoporous cristobalite.[6]

3.4. Epitaxial Relationships

Silica films in contact with Si-(100) demonstrate mono-oriented α-quartz upon MIC (Figure 9).[3] The crystalline substrate may suppress the formation of silicates and crystal phases other than α-quartz, which are otherwise observed.[2] The crystallization is not induced by the epitaxial relationship, but the crystal phase and orientation are selected by the substrate.

3.5. Maintaining Structure during Crystallization

Thanks to MIC, we were able to produce the first quartz-based nanomaterials on a substrate via a bottom-up synthesis (Figure 10).[3] Silica with three different pore morphologies spanning from mesopores to macropores were prepared and then crystallized on a silicon substrate using either Sr^{2+} or Ba^{2+} to induce crystallization. Crystallization started in the silica top-layer and, then, propagated into the silicon substrate as the substrate oxidized, creating a quartz layer of tunable thickness. The macropores and the larger mesopores of ∼30 nm maintained their structure upon crystallization, whereas the smaller mesopores produced crystal domains with a trapezoidal habit.

To probe the range of mesopores that could be retained, we used several PB−PEO diblock copolymers as templating agents to make amorphous silica films with varying wall thicknesses and mesopore diameters (Figure 11). These were then crystallized by infiltrating the mesopores with an alkaline earth metal salt and heating in a furnace. Pores larger than 25 nm were retained upon crystallization.[47] In samples where the mesoporosity was preserved upon crystallization, the d-spacing of the original silica film was maintained (Figure 11). Typically, mesopore structures are lost during the crystallization of silica due to the relatively slow nucleation rate followed by the extremely fast growth rate of quartz,[48] which generates crystallites much larger than the original pore structures. However, we have observed that the MIC method

https://doi.org/10.1021/acs.accounts.1c00592
Acc. Chem. Res. XXXX, XXX, XXX−XXX

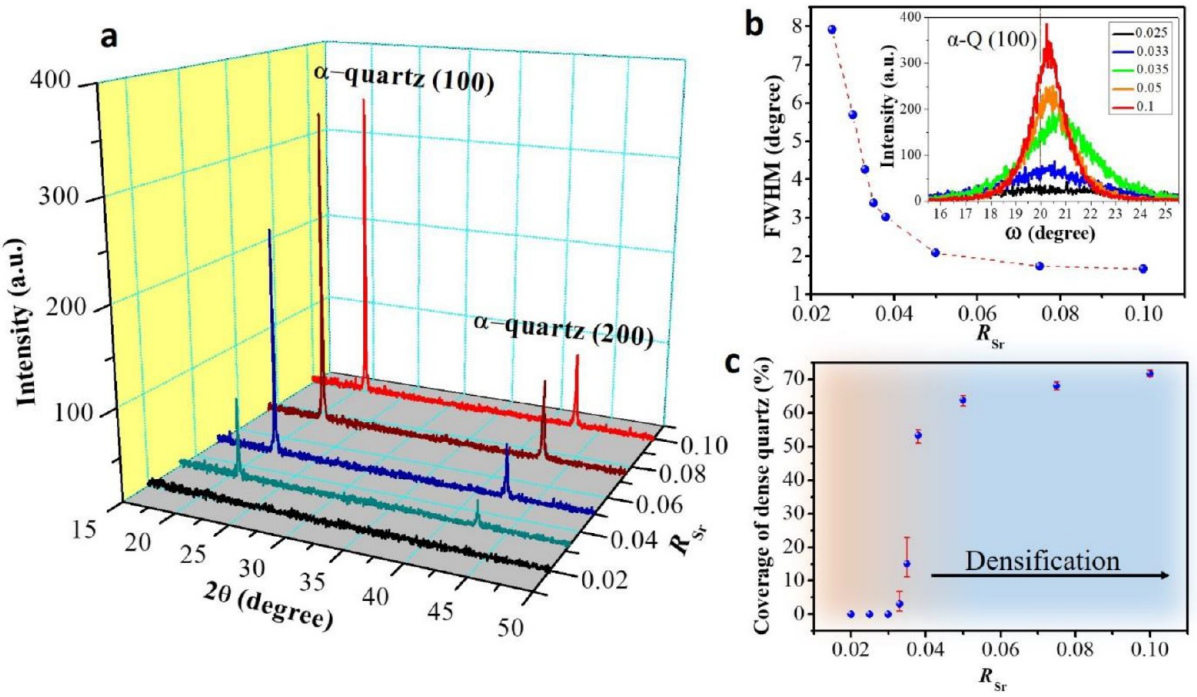

Figure 6. (a) XRD θ–2θ scan results of epitaxial quartz films with different Sr/SiO_2 ratios (R_{Sr}). (b) Relationship between the fwhm of rocking curves of α-quartz (100) and R_{Sr}. (c) Influence of R_{Sr} on the area covered by α-quartz. Adapted with permission from ref 45. Copyright 2019. Accessible via the Royal Society of Chemistry Creative Commons Attribution 3.0.

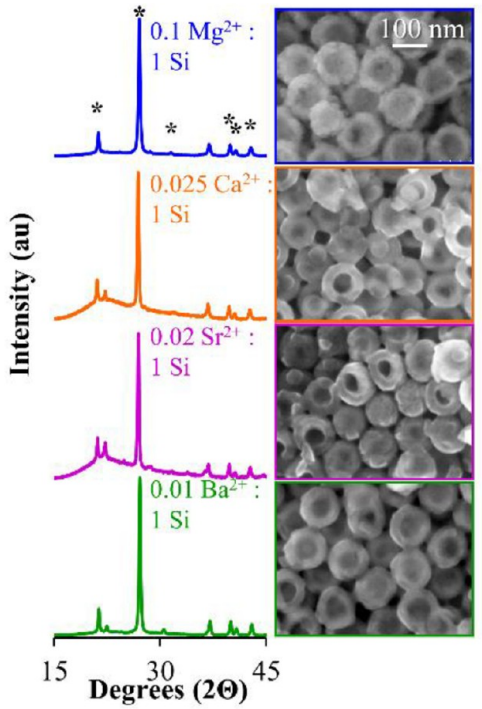

Figure 7. Diffractograms and corresponding SEM images of hollow quartz spheres produced from different alkaline earth devitrification agents. Adapted with permission from ref 2. Copyright 2015 The Royal Society of Chemistry.

often generates smaller crystallite sizes than those produced via high temperature calcination.

In addition to curvature, wall thickness also likely affects the ability to conserve the mesopore structure during crystallization. Thus, we studied whether or not very thin walls (10 nm) permitted structural preservation during MIC.[2] In the absence of mesoporosity, the heat treatment time needed to be tripled to achieve crystallization. However, even with SiO_2 wall thicknesses below 10 nm, the macropore structure remained upon transformation into a crystalline phase.

We further studied morphological preservation in structured nanoparticles here, exploring the impact of the metal ion radius on crystallization behavior (Figure 12).[2] During the crystallization process, the mesopores in the silica wall, having a diameter of several nanometers, lost their structure to produce a densified 20 nm shell around a hollow center (~80 nm). The progressive collapse of the mesoporosity with increasing treatment temperature can be observed in the SEM micrographs and in the disappearance of a hysteresis loop in the nitrogen adsorption–desorption experiments (Figure 12). The shell was polycrystalline with the average crystallite size depending on the treatment temperature.

3.6. Material Fabrication

The major advantage of MIC is the ability to retain a complex and delicate morphology upon crystallization. Putz et al. were able to 3D print hierarchically porous silica into a lattice-like scaffold structure.[44] The mesoporosity was then infiltrated using a $MgCl_2$ solution and then calcined, crystallizing to α-quartz (Figure 13).

The MIC of silica films leads to epitaxial crystallization of the silica phase thanks to the small mismatch with the crystalline silicon substrate. Patterned substrates are no different. Zhang et al. have shown that silica xerogels containing a small amount of $SrCl_2$ can be patterned using soft imprint lithography (Figure 14).[45] All of the pillars produced on the substrate contained the same crystallographic phase. There are other methods to micropattern quartz surfaces, and of these, the thinnest quartz crystals are about

https://doi.org/10.1021/acs.accounts.1c00592
Acc. Chem. Res. XXXX, XXX, XXX–XXX

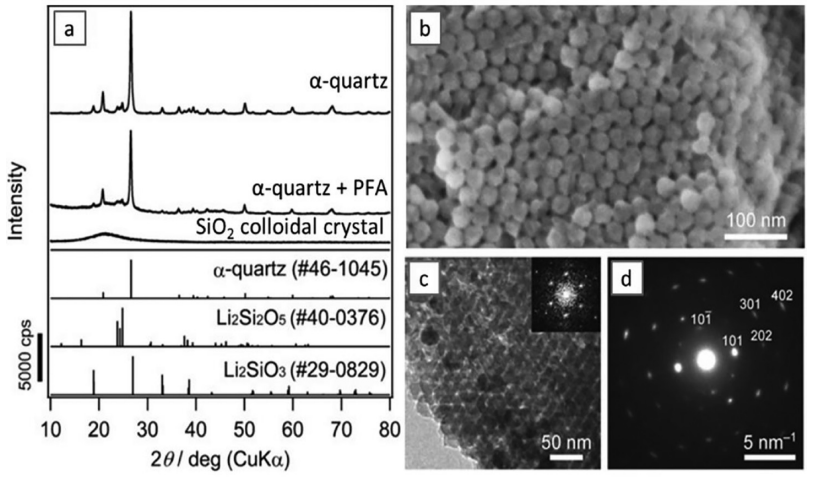

Figure 8. (a) Diffractograms and corresponding (b) SEM, (c) TEM, and (d) selected area electron diffraction images of monocrystalline hollow quartz spheres. Adapted with permission from ref 43. Copyright 2016. Accessible via Wiley/VCH Creative Commons Attribution 4.0.

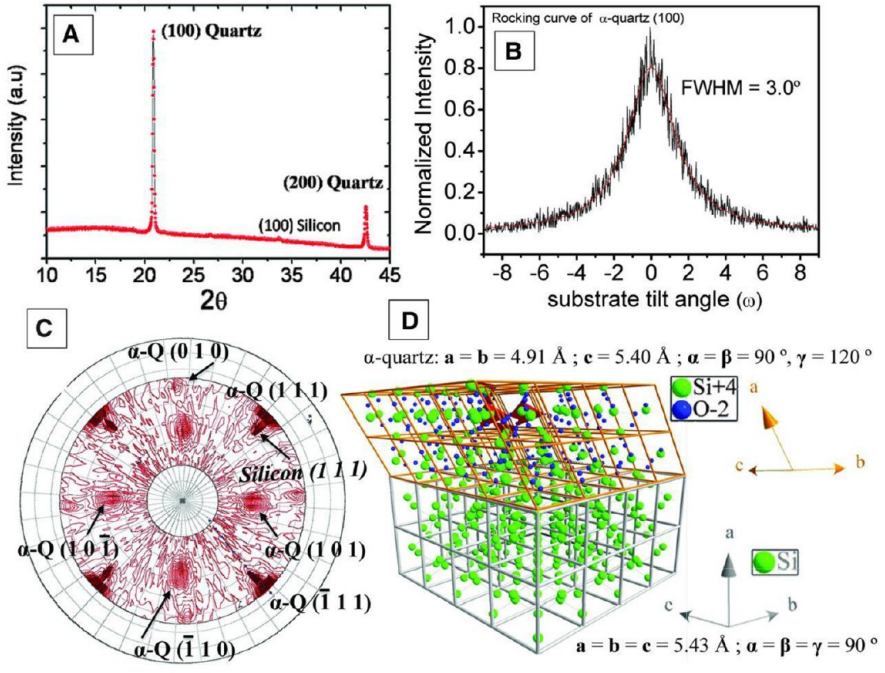

Figure 9. Crystallinity in a macroporous quartz film after MIC using strontium, as shown using (A) X-ray diffraction, (B) a rocking curve, and (C) a pole figure. (D) The epitaxial relationship between the silicon substrate (in gray) and the α-quartz film (in orange) is depicted using a 3D ball-and-stick model. Reproduced with permission from ref 3. Copyright 2013 AAAS.

10 μm.[49] However, when a patterned silica film is crystallized using MIC, α-quartz films as thin as 200 nm are possible, allowing the operating frequency of the material to be 50 times higher than previously fabricated devices.[49]

The ability to retain the mesostructure and use epitaxy to select for a particular phase orientation is interesting in terms of the piezoelectric properties of silica. The piezoelectric response in α-quartz films can be measured using piezoelectric force microscopy[4] and direct piezoelectric force microscopy.[50] When direct piezoelectric force microscopy was used, the first direct measurement of the d_{33} piezoelectric coefficient in these epitaxial quartz thin films was made.[45] The piezoelectric response was similar to bulk crystals and homogeneous irrespective of the macrostructuration, demonstrating structural and functional homogeneity within films grown by MIC.

3.7. Applications

The integration of piezoelectric quartz onto silicon in the single crystalline form can trigger development in sensors.[51] Quartz finds a place in many application areas, ranging from biology to electronics. Its nanostructuration receives attention due to its piezoelectricity and biocompatibility. However, the current techniques for quartz-based devices on silicon substrates are limited in terms of device thickness and their integration, which directly affects the overall performance and increases the integration cost. Thanks to the MIC of sol−gel silica films combined with nanoimprint lithography and microfabrication techniques, the first α-quartz (100)-based microcantilever device was fabricated on a silicon−insulator−silicon (SOI) (100) substrate (Figure 15).[52,53] The parameters that directly affect the device performance, such as the crystal

https://doi.org/10.1021/acs.accounts.1c00592
Acc. Chem. Res. XXXX, XXX, XXX−XXX

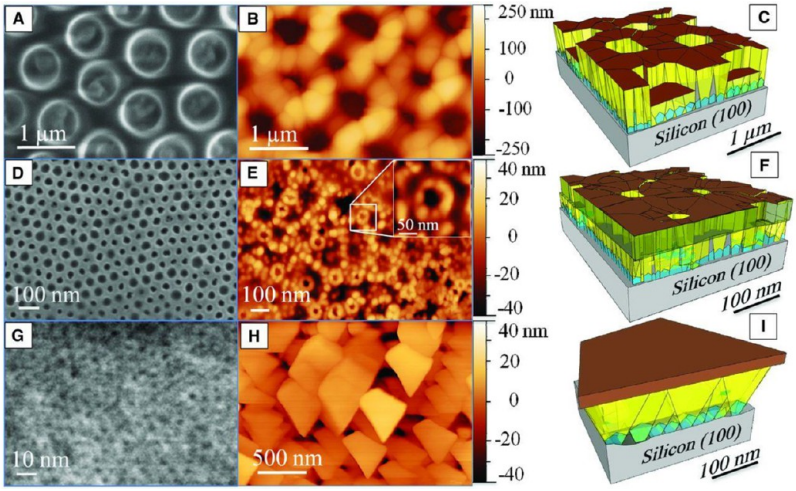

Figure 10. (A, D, G) SEM images of amorphous silica films and (B, E, H) AFM images of crystalline α-quartz structured thin films after the MIC. (C, F, I) Diagram of the morphology of the crystalline thin film. Reproduced with permission from ref 3. Copyright 2013 AAAS.

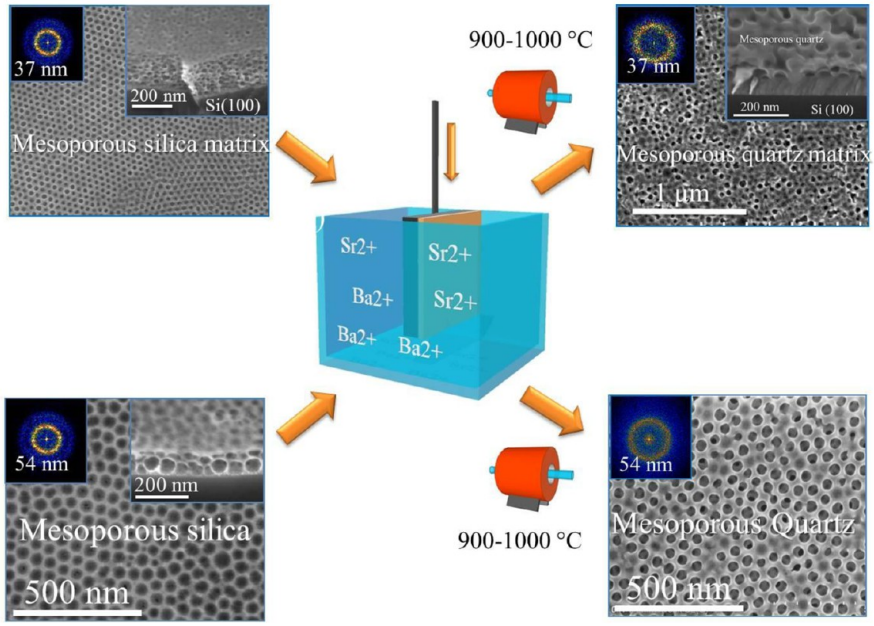

Figure 11. Large mesopores remain intact upon MIC using either Ba^{2+} or Sr^{2+} of structured silica films. Reproduced with permission from ref 47. Copyright 2014 The Royal Society of Chemistry.

quality, piezoelectric functionality, and quality factor of the quartz, were preserved during the microfabrication process. These ultrasensitive quartz devices are capable of measuring tiny masses (<10 pg) or forces through a variation in the resonant frequency.

4. OTHER OXIDES

4.1. Alumina

Alumina is an important material possessing several crystalline phases of different chemical, electrical, and mechanical properties. Among them, α-alumina is stable at high temperatures and therefore widely used in modern industries. It is usually prepared by the first dehydration of amorphous alumina at 500 °C to form γ-alumina, followed by an annealing step at 1100 °C. The temperature of the γ-to-α transition can be influenced by some cation additives. Although some cations were found to accelerate the transition (Fe^{2+}, Cu^{2+}, Mn^{2+}, Cr^{3+}, or Ti^{4+}),[54−57] most cations, such as the monovalent (Li^+, Na^+, Ag^+, K^+, Rb^+, and Cs^+)[58,59] or divalent cations (Co^{2+}, Ni^{2+}, Mg^{2+}, Ca^{2+}, Sr^{2+}, and Ba^{2+}), had no effect or retarded the transition.[56]

It has been reported that the addition of small amounts of specific fluoride salts can decrease the polymorphous transformation temperature of the α-Al_2O_3 phase. Živkovic et al. showed that the addition of 2% fluoride using AlF_3, MgF_2, and CaF_2 decreased the crystallization temperature by up to 400 °C, whereas alkali fluoride salts (NaF, LiF, and Na_3AlF_6) did not impact the phase transition of aluminum oxide.[60] Whereas Wu et al. found AlF_3 and ZnF_2 to be effective accelerating agents for the gamma to alpha phase transformation,[57] Li et al. found contradictory results: LiF and AlF_3 were capable of inducing Al_2O_3 crystallization at a much lower temperature than the pure oxide, but ZnF_2 did not.[61] Choi et al. later expanded the study of fluoride salts, adding chloride salts to

https://doi.org/10.1021/acs.accounts.1c00592
Acc. Chem. Res. XXXX, XXX, XXX−XXX

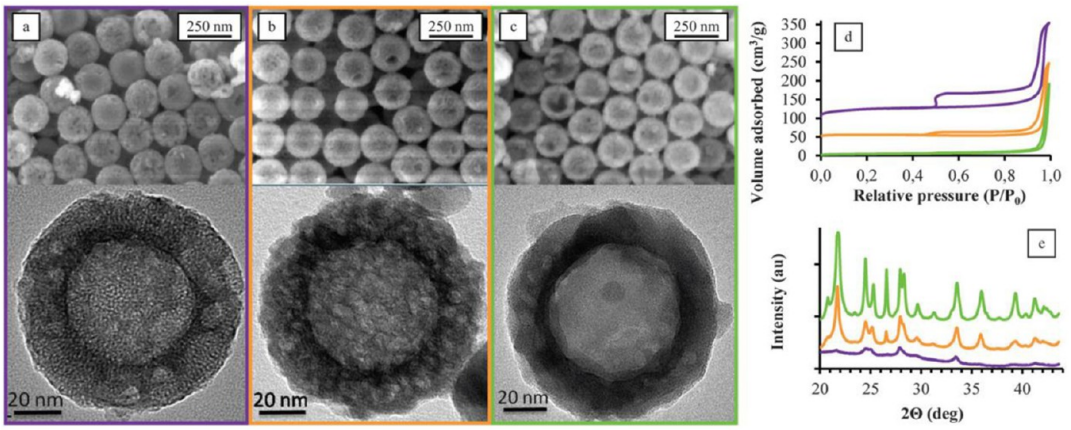

Figure 12. SEM (above) and TEM (below) micrographs of hollow amorphous silica spheres previously soaked in alkaline metal salt and calcined for 5 h under air at (a) 800 °C (purple), (b) 900 °C (orange), and (c) 1000 °C (green). (d) Nitrogen sorption isotherms of particles calcined at 800, 900, and 1000 °C. (e) X-ray diffraction patterns showing the change in pattern intensity with crystallization temperature. Reproduced with permission from ref 2. Copyright 2015 The Royal Society of Chemistry.

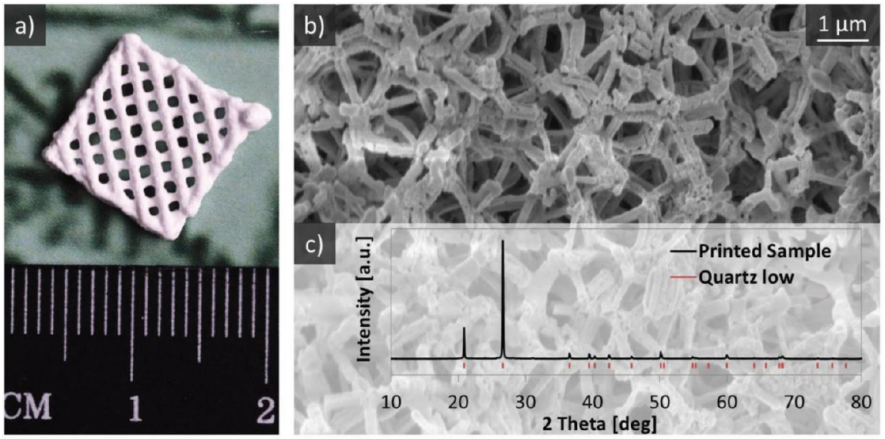

Figure 13. (a) Low quartz printed into a 3D scaffold. (b) Retention of the macroporous network upon crystallization. (c) X-ray diffraction of the crystalline scaffold. Reproduced with permission from ref 44. Copyright 2018. Accessible via Wiley/VCH Creative Commons Attribution 4.0.

the devitrification agent mixture.[62] In the case of sodium ions, the chloride salts promoted larger and more homogeneous crystal growth.

4.2. Semiconductor Oxides

Amorphous semiconductor oxides, such as $ZnSnO_3$ (ZTO), InGaZnO (IGZO), and InGaO (IGO), have attracted considerable attention as an alternative to current silicon-based semiconductors due to their superior properties, such as high mobility, low-temperature fabrication, good transparency, and a low leakage current. They have been widely used as key elements of versatile optoelectronics and are promising candidates for active materials for high-performance thin-film transistors. However, crystalline oxide semiconductors are more performant and more likely to meet the requirements of next-generation optoelectronics, such as higher field effect mobility. Recently, Jeong's group demonstrated that the MIC processes of vacuum-deposited amorphous semiconductors yield high-quality crystalline $ZnSnO_3$ semiconductors at low temperatures (Figure 16a).[63] This achievement was obtained by applying a tantalum metal capping layer to the back surface of the metal oxide. During the annealing process, the Ta film oxidizes to form TaOx and releases electrons to the underlying layer. These electrons weaken the metal oxide bonds. The bonds eventually break and reform into a crystalline phase (Figure 16b). The approach was successfully extended to other oxide semiconductors, such as InGaZnO,[64] ZnON,[65] and IGO.[66] They all exhibit improved performances and long-term stability, thanks to the tantalum oxide layer encapsulation, for applications in the display industry and flash memory application.[67]

4.3. Ni_xO, TiO_x, and SnO_x

During an attempt to incorporate a Ni_xO hole-transporting layer into hybrid organic−inorganic perovskite solar cells, Hou et al. discovered that the sintering temperature of a Ni_xO layer could be lowered by 100 °C by embedding it in a Au phase.[35] The metal not only induces amorphous-to-crystalline physical transformation but also catalyzes the condensation of the sol−gel precursors. MIC was shown to occur in a variety of sol−gel materials, including Ni_xO using either Au or Ag; TiO_x using Ni, Au, or Pt; SnO_x using Ni.

4.4. $LiCoO_2$

$LiCoO_2$ is the most widely used cathode material in thin film batteries, which is usually fabricated as amorphous thin films requiring heat treatment to crystallize and function optimally. Complete crystallization is achieved at 700 °C, which is too high for microelectronics. Cho et al. prepared $LiCoO_2$ thin

https://doi.org/10.1021/acs.accounts.1c00592
Acc. Chem. Res. XXXX, XXX, XXX−XXX

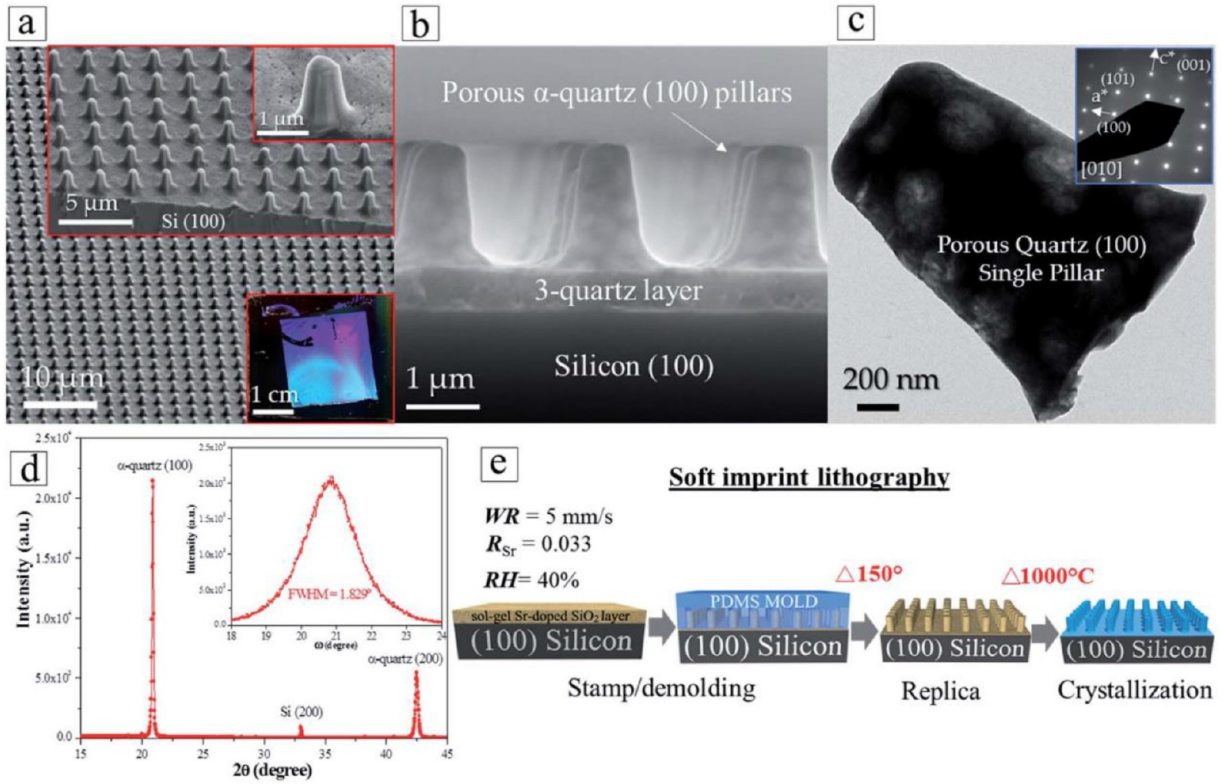

Figure 14. (a, b) Crystallized, epitaxial α-quartz pillars organized on a silicon substrate produced using soft imprint lithography. (c) TEM image and electron diffraction of a monocrystalline pillar. (d) X-ray diffractogram showing the (100) α-quartz crystallographic orientation. (e) Synthetic protocol. Reproduced with permission from ref 45. Copyright 2019. Accessible via the Royal Society of Chemistry Creative Commons Attribution 4.0.

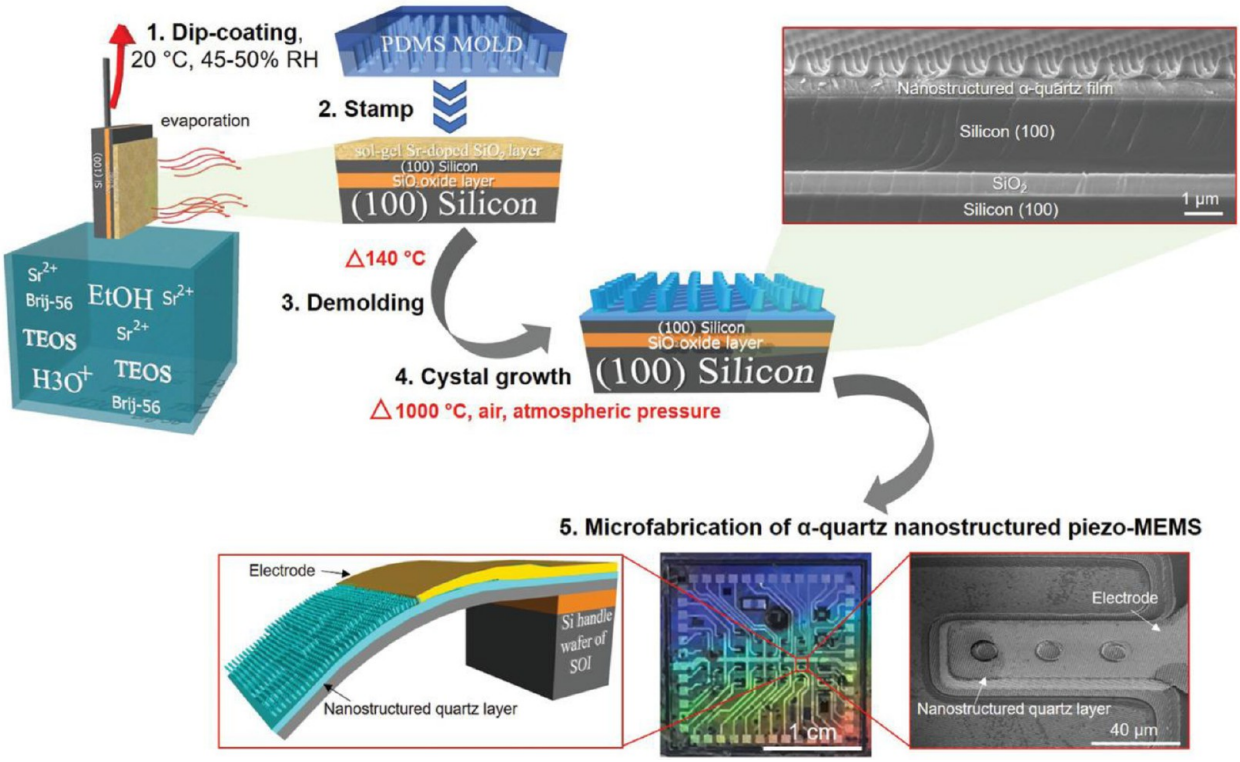

Figure 15. General schematic of the microfabrication steps of piezoelectric nanostructured epitaxial quartz-based micro- and nano-electromechanical devices. Reproduced with permission from ref 53. Copyright 2021. Accessible via Wiley/VCH Creative Commons Attribution 4.0.

https://doi.org/10.1021/acs.accounts.1c00592
Acc. Chem. Res. XXXX, XXX, XXX−XXX

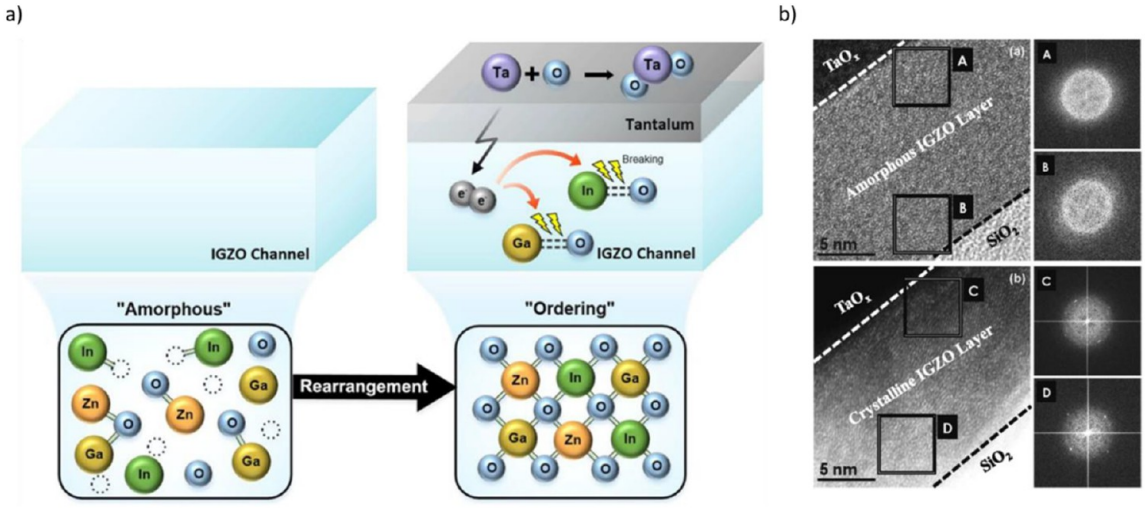

Figure 16. (a) Representation of the IGZO crystallization mechanism induced by a Ta layer. (b) Cross-sectional TEM images of the IGZO layer with the Ta layer after thermal annealing layer after thermal annealing at (top) 200 °C and (bottom) 300 °C under an O_2 atmosphere. Selected area electron diffraction patterns near the top and bottom interface are shown in the insets. Adapted with permission from ref 64. Copyright 2017. Accessible via Springer Creative Commons Attribution 4.0.

films by deposition using magnetron sputtering.[68] They demonstrated that the Al-induced crystallization of $LiCoO_2$ was achieved at 600 °C and showed better structural and electrochemical properties than the reference.

4.5. MoO_3

Cheyns et al. demonstrated that MoO_3 thin films could be used as thickness-tunable transport layers in organic photovoltaics if doped with small amounts of metal.[69] The samples were prepared by thermal evaporation and deposition on a substrate without annealing. The improved crystallinity enhanced the conductivity with the onset crystallization temperature being reduced from 450 °C to approximately room temperature.

Seeing the diversity of systems that respond to MIC, we can conclude that this is a very generalizable phenomenon. It is worth doing further research to optimize the crystallization temperature, the degree of crystallinity, and the phase control to better increase material performance and to produce crystalline temperature-sensitive hybrid and composite materials.

5. CONCLUSIONS AND PERSPECTIVES

MIC is a powerful tool to crystallize amorphous materials at low temperature and tackle industrial challenges. It is still a growing domain in metal oxides, despite its large spread usage in silicon and germanium crystallization. The basis of the MIC method is that metal cations result in the recombination of oxide bonds and a large variety of cations can be used as devitrification agents; however, the optimum concentration varies as a function of cation size and oxidation state and the metal oxide. Different cations affect the temperature of crystallization, the size of crystal domains, and the crystalline phase(s) obtained. Mixtures of cations can provide fine control over the mix of different crystal phases.[70] However, the mechanisms involved in MIC are not yet well enough understood to have a model that predicts the effects of a given cation on the crystallization temperature of a given oxide. Many different techniques can be used to provide the energy needed for the phase transformation, including microwaves, sonochemistry, lasers, and classical calcination methods. It is possible that, in some of these techniques, a mixture of crystallization mechanisms occurs simultaneously, for instance, dissolution−reprecipitation of crystalline phases in tandem with MIC.

One aspect that still needs to be examined is crystal nucleation and growth during MIC. There are some instances where a film or a nanosized object is either perfectly crystalline or completely amorphous. We have observed this occurrence in thin films where a certain percentage does not crystallize upon heat treatment, while others are completely crystalline across the entire thin film.[71] The same is visible in batches of particles where some are crystalline while others remain amorphous.[1,41]

Future research will certainly focus on hybrid and composite materials. For instance, a metal oxide could be crystallized on heat sensitive plastic substrates,[25] or crystallization could be induced at low temperature in the presence of metals, circumventing metal melting and dewetting.

AUTHOR INFORMATION

Corresponding Authors

Clément Sanchez − *Laboratoire Chimie de la Matière Condensée, UMR 7574, Sorbonne Université-Collège de France-CNRS, 75005 Paris, France;* orcid.org/0000-0002-6426-4844; Email: clement.sanchez@upmc.fr

Glenna L. Drisko − *CNRS, Univ. Bordeaux, Bordeaux INP, ICMCB, F-33600 Pessac, France;* orcid.org/0000-0001-6469-9736; Phone: +33 5 40 00 26 68; Email: glenna.drisko@icmcb.cnrs.fr

Authors

Laurent Lermusiaux − *Univ. Lyon, CNRS, École Normale Supérieure de Lyon, Laboratoire de Chimie, UMR 5182, F-69007 Lyon, France;* orcid.org/0000-0003-3024-0649

Antoine Mazel − *CNRS, Univ. Bordeaux, Bordeaux INP, ICMCB, F-33600 Pessac, France*

Adrian Carretero-Genevrier − *Institut d'Electronique et des Systèmes (IES), CNRS, Université de Montpellier,*

https://doi.org/10.1021/acs.accounts.1c00592
Acc. Chem. Res. XXXX, XXX, XXX−XXX

Montpellier 34095, France; orcid.org/0000-0003-0488-9452

Complete contact information is available at: https://pubs.acs.org/10.1021/acs.accounts.1c00592

Notes

The authors declare no competing financial interest.

Biographies

Laurent Lermusiaux currently works as a postdoc at the Laboratoire de Chimie of the Ecole Normale Supérieure de Lyon. He obtained his Ph.D. from Sorbonne University in 2015. He then performed postdoctorates at Monash University and the ICMCB. His scientific interests cover synthesis, self-assembly, and characterization of hybrid nanoparticles.

Antoine Mazel obtained his Ph.D. in 2018 from the University of Nantes, followed by a postdoc at the ICMCB where he specialized in silicon chemistry and MIC of oxides. His research interests are at the interface of synthetic organic, inorganic, and hybrid materials chemistry.

Adrian Carretero-Genevrier has been a CNRS Researcher at the IES since 2016, where he leads the nanochemistry group (www.nanochemlab.com). He obtained his Ph.D. in 2010 in Materials Science from the Universitat Autònoma de Barcelona and then conducted a postdoc at the LCMCP. His research aims to understand the growth mechanisms of functional oxide nanostructures synthesized by soft chemistry and to integrate sensing and harvesting energy functionalities into MEMS and other resonant systems. He has been awarded a Starting Grant from the European Research Council, the young researcher award (ANR JCJC), and the outstanding Award for a Ph.D. in Materials Science.

Clément Sanchez is an Emeritus Professor at the Collège de France and chair of Chemistry of Hybrid Materials. He was the director of The Laboratoire de Chimie de la Matière Condensée de Paris from 1999 to 2013. He received a Ph.D. in physical chemistry from the University of Paris VI in 1981. He has a chair position at the Institut of Advanced Study of the University of Strasbourg (Chair of chemistry of ultradivided matter, 2020−2021, USIAS) and at the ICMCB. He specializes in the field of nanochemistry and physical properties of nanostructured porous and nonporous transition metal oxide-based gels and hybrid organic−inorganic materials in the form of monoliths, microspheres, and films.

Glenna L. Drisko pursued her doctorate at The University of Melbourne, studying the control of pore structures in metal oxides. She performed a postdoctorate at the LCMCP, where she first learned about MIC. Upon becoming a CNRS research scientist in the ICMCB in 2017, she continued studying sol−gel synthetic processes, crystallization, and fabrication of optical metamaterials from crystalline dielectric particles. She has been awarded the L'Oreal/Unesco award for Women in Science. She launched her independent career via a Junior Chair, which was followed by funding from an ERC starting grant entitled *Scatter* (https://glennadrisko.com/).

■ ACKNOWLEDGMENTS

G.L.D. received funding for this work from the European Research Council (ERC) under the European Union's Horizon 2020 research and innovation programme (Grant agreement No. 948319). A.M. and G.L.D. were supported by the LabEx AMADEus (ANR-10-LABX-42) in the framework of IdEx Bordeaux (ANR-10-IDEX-03-02), i.e., the Investissements d'Avenir program of the French government managed by the Agence Nationale de la Recherche. A.C.-G. acknowledges the European Research Council (ERC) under the European Union's Horizon 2020 Research and Innovation Programme (project SENSiSOFT No. 803004) for financial support. C.S. thanks Université de Bordeaux and Laboratories and its Labex for support.

■ ABBREVIATIONS

EDX, energy-dispersive X-ray spectroscopy; SAED, selected area electron diffraction; PB−PEO, poly(butadiene−ethylene oxide); TEM, transmission electron microscopy; SEM, scanning electron microscopy; XRD, X-ray diffraction

■ REFERENCES

(1) Danty, P. M. P.; Mazel, A.; Cormary, B.; De Marco, M. L.; Allouche, J.; Flahaut, D.; Jimenez-Lamana, J.; Lacomme, S.; Delville, M.-H.; Drisko, G. L. Microwave-Assisted and Metal-Induced Crystallization: A Rapid and Low Temperature Combination. *Inorg. Chem.* **2020**, *59* (9), 6232−6241.

(2) Drisko, G. L.; Carretero-Genevrier, A.; Perrot, A.; Gich, M.; Gàzquez, J.; Rodriguez-Carvajal, J.; Favre, L.; Grosso, D.; Boissière, C.; Sanchez, C. Crystallization of Hollow Mesoporous Silica Nanoparticles. *Chem. Commun.* **2015**, *51* (20), 4164−4167.

(3) Carretero-Genevrier, A.; Gich, M.; Picas, L.; Gazquez, J.; Drisko, G. L.; Boissiere, C.; Grosso, D.; Rodriguez-Carvajal, J.; Sanchez, C. Soft-Chemistry−Based Routes to Epitaxial α-Quartz Thin Films with Tunable Textures. *Science* **2013**, *340* (6134), 827−831.

(4) Drisko, G. L.; Carretero-Genevrier, A.; Gich, M.; Gàzquez, J.; Ferrah, D.; Grosso, D.; Boissière, C.; Rodriguez-Carvajal, J.; Sanchez, C. Water-Induced Phase Separation Forming Macrostructured Epitaxial Quartz Films on Silicon. *Adv. Funct. Mater.* **2014**, *24* (35), 5494−5502.

(5) Venezia, A. M.; La Parola, V.; Longo, A.; Martorana, A. Effect of Alkali Ions on the Amorphous to Crystalline Phase Transition of Silica. *J. Solid State Chem.* **2001**, *161* (2), 373−378.

(6) Matsuno, T.; Nakaya, T.; Kuroda, Y.; Wada, H.; Shimojima, A.; Kuroda, K. Synthesis of Cristobalite Containing Ordered Interstitial Mesopores Using Crystallization of Silica Colloidal Crystals. *Chem. - Asian J.* **2021**, *16* (3), 207−214.

(7) Wang, Z.; Jeurgens, L. P. H.; Mittemeijer, E. J. *Metal-Induced Crystallization Fundamentals and Applications*; Pan Stanford Publishing, 2015.

(8) Bassett, D. R.; Boucher, E. A.; Zettlemoyer, A. C. The Effect of Alkali Halides and Silver Nitrate on the Crystallization of Silica Powders. *J. Mater. Sci.* **1972**, *7* (12), 1379−1382.

(9) Brun, A. *Arch. Sci. Phys. Nat.* **1908**, *25*, 610.

(10) De Marco, M. L.; Semlali, S.; Korgel, B. A.; Barois, P.; Drisko, G. L.; Aymonier, C. Silicon-Based Dielectric Metamaterials: Focus on the Current Synthetic Challenges. *Angew. Chem., Int. Ed.* **2018**, *57* (17), 4478−4498.

(11) Ohtani, B.; Ogawa, Y.; Nishimoto, S. Photocatalytic Activity of Amorphous−Anatase Mixture of Titanium(IV) Oxide Particles Suspended in Aqueous Solutions. *J. Phys. Chem. B* **1997**, *101* (19), 3746−3752.

(12) Uboldi, C.; Urbán, P.; Gilliland, D.; Bajak, E.; Valsami-Jones, E.; Ponti, J.; Rossi, F. Role of the Crystalline Form of Titanium Dioxide Nanoparticles: Rutile, and Not Anatase, Induces Toxic Effects in Balb/3T3Mouse Fibroblasts. *Toxicol. In Vitro* **2016**, *31*, 137−145.

(13) Bouajaj, A.; Ferrari, M.; Montagna, M. Crystallization of Silica Xerogels: A Study by Raman and Fluorescence Spectroscopy. *J. Sol-Gel Sci. Technol.* **1997**, *8* (1), 391−395.

(14) Oki, F.; Ogawa, Y.; Fujiki, Y. Effect of Deposited Metals on the Crystallization Temperature of Amorphous Germanium Film. *Jpn. J. Appl. Phys.* **1969**, *8* (8), 1056.

(15) Bosnell, J. R.; Voisey, U. C. The Influence of Contact Materials on the Conduction Crystallization Temperature and Electrical Properties of Amorphous Germanium, Silicon and Boron Films. *Thin Solid Films* **1970**, *6* (3), 161−166.
(16) Garníca-Romo, M. G.; González-Hernández, J.; Hernández-Landaverde, M. A.; Vorobiev, Y. V.; Ruiz, F.; Martínez, J. R. Structure of Heat-Treated Sol-Gel SiO2 Glasses Containing Silver. *J. Mater. Res.* **2001**, *16* (7), 2007−2012.
(17) Haro-Poniatowski, E.; Vargas-Muños, S.; Arroyo-Murillo, R.; Rodríguez-Talavera, R.; Diamant, R. Laser-Induced Crystallization of Co(II)-Doped Titania. *Mater. Res. Bull.* **1996**, *31* (3), 329−334.
(18) Zhang, Y.; Li, J.; Wang, J. Substrate-Assisted Crystallization and Photocatalytic Properties of Mesoporous TiO2 Thin Films. *Chem. Mater.* **2006**, *18* (12), 2917−2923.
(19) Perkas, N.; Pol, V. G.; Pol, S. V.; Gedanken, A. Gold-Induced Crystallization of SiO2 and TiO2 Powders. *Cryst. Growth Des.* **2006**, *6* (1), 293−296.
(20) Hanaor, D. A. H.; Sorrell, C. C. Review of the Anatase to Rutile Phase Transformation. *J. Mater. Sci.* **2011**, *46* (4), 855−874.
(21) Debeila, M. A.; Raphulu, M. C.; Mokoena, E.; Avalos, M.; Petranovskii, V.; Coville, N. J.; Scurrell, M. S. The Effect of Gold on the Phase Transitions of Titania. *Mater. Sci. Eng., A* **2005**, *396* (1), 61−69.
(22) Zhang, Y.-H.; Reller, A. Phase Transformation and Grain Growth of Doped Nanosized Titania. *Mater. Sci. Eng., C* **2002**, *19* (1), 323−326.
(23) Vargas, S.; Arroyo, R.; Haro, E.; Rodríguez, R. Effects of Cationic Dopants on the Phase Transition Temperature of Titania Prepared by the Sol-Gel Method. *J. Mater. Res.* **1999**, *14* (10), 3932−3937.
(24) Mosquera, A. A.; Albella, J. M.; Navarro, V.; Bhattacharyya, D.; Endrino, J. L. Effect of Silver on the Phase Transition and Wettability of Titanium Oxide Films. *Sci. Rep.* **2016**, *6* (1), 32171.
(25) Yang, C.; Hirose, Y.; Nakao, S.; Hoang, N. L. H.; Hasegawa, T. Metal-Induced Solid-Phase Crystallization of Amorphous TiO2 Thin Films. *Appl. Phys. Lett.* **2012**, *101* (5), No. 052101.
(26) Yang, C.; Hirose, Y.; Nakao, S.; Hasegawa, T. TiO2 Thin Film Crystallization Temperature Lowered by Cu-Induced Solid Phase Crystallization. *Thin Solid Films* **2014**, *553*, 17−20.
(27) Sangani, L. D. V.; Sri, K. V.; Mohiddon, M. A.; Krishna, M. G. Low Temperature Au Induced Crystallization of Titanium Dioxide Thin Films for Resistive Switching Applications. *RSC Adv.* **2015**, *5* (83), 67493−67499.
(28) Hultman, L.; Robertsson, A.; Hentzell, H. T. G.; Engström, I.; Psaras, P. A. Crystallization of Amorphous Silicon during Thin-film Gold Reaction. *J. Appl. Phys.* **1987**, *62* (9), 3647−3655.
(29) Nair, J.; Nair, P.; Mizukami, F.; Oosawa, Y.; Okubo, T. Microstructure and Phase Transformation Behavior of Doped Nanostructured Titania. *Mater. Res. Bull.* **1999**, *34* (8), 1275−1290.
(30) Doeuff, S.; Henry, M.; Sanchez, C.; Livage, J. The Gel Route to Cr3+-Doped TiO2, an ESR Study. *J. Non-Cryst. Solids* **1987**, *89* (1), 84−97.
(31) Camacho-López, M. A.; Vargas, S.; Arroyo, R.; Haro-Poniatowski, E.; Rodríguez, R. Raman Studies on Laser Induced Crystallization of Co(II) Doped Titania; Effect of the Dopant Concentration. *Opt. Mater.* **2002**, *20* (1), 43−50.
(32) García-Serrano, J.; Gómez-Hernández, E.; Ocampo-Fernández, M.; Pal, U. Effect of Ag Doping on the Crystallization and Phase Transition of TiO2 Nanoparticles. *Curr. Appl. Phys.* **2009**, *9* (5), 1097−1105.
(33) Akgun, B. A.; Durucan, C.; Mellott, N. P. Effect of Silver Incorporation on Crystallization and Microstructural Properties of Sol−Gel Derived Titania Thin Films on Glass. *J. Sol-Gel Sci. Technol.* **2011**, *58* (1), 277−289.
(34) Amarjargal, A.; Tijing, L. D.; Kim, C. S. Effect of Annealing on the Phase Transition and Morphology of Ag NPs on/in TiO2 Rods Synthesized by a Polyol Method. *Ceram. Int.* **2012**, *38* (8), 6365−6375.
(35) Hou, C.-H.; Shyue, J.-J.; Su, W.-F.; Tsai, F.-Y. Catalytic Metal-Induced Crystallization of Sol−Gel Metal Oxides for High-Efficiency Flexible Perovskite Solar Cells. *J. Mater. Chem. A* **2018**, *6* (34), 16450−16457.
(36) Rodríguez-Talavera, R.; Vargas, S.; Arroyo-Murillo, R.; Montiel-Campos, R.; Haro-Poniatowski, E. Modification of the Phase Transition Temperatures in Titania Doped with Various Cations. *J. Mater. Res.* **1997**, *12* (2), 439−443.
(37) Shin, J. C.; Kwon, S. M.; Kang, J.; Jeon, S. P.; Heo, J.-S.; Kim, Y.-H.; Cho, S. W.; Park, S. K. Catalytic Metal-Accelerated Crystallization of High-Performance Solution-Processed Earth-Abundant Metal Oxide Semiconductors. *ACS Appl. Mater. Interfaces* **2020**, *12* (22), 25000−25010.
(38) Zhao, J.; Sallard, S.; Smarsly, B. M.; Gross, S.; Bertino, M.; Boissière, C.; Chen, H.; Shi, J. Photocatalytic Performances of Mesoporous TiO2 Films Doped with Gold Clusters. *J. Mater. Chem.* **2010**, *20* (14), 2831−2839.
(39) Roccaforte, F.; Bolse, W.; Lieb, K. P. Solid Phase Epitaxial Regrowth of Ion Beam-Amorphized α-Quartz. *Appl. Phys. Lett.* **1998**, *73* (10), 1349−1351.
(40) Gustafsson, M.; Roccaforte, F.; Keinonen, J.; Bolse, W.; Ziegeler, L.; Lieb, K. P. Oxygen-Activated Epitaxial Recrystallization of Li-Implanted α-SiO2. *Phys. Rev. B: Condens. Matter Mater. Phys.* **2000**, *61* (5), 3327−3332.
(41) Okabayashi, M.; Miyazaki, K.; Kono, T.; Tanaka, M.; Toda, Y. Preparation of Spherical Particles with Quartz Single Crystal. *Chem. Lett.* **2005**, *34* (1), 58−59.
(42) Yin, H.; Ma, Z.; Zhu, H.; Chi, M.; Dai, S. Evidence for and Mitigation of the Encapsulation of Gold Nanoparticles within Silica Supports upon High-Temperature Treatment of Au/SiO2 Catalysts: Implication to Catalyst Deactivation. *Appl. Catal., A* **2010**, *386* (1), 147−156.
(43) Matsuno, T.; Kuroda, Y.; Kitahara, M.; Shimojima, A.; Wada, H.; Kuroda, K. A Single-Crystalline Mesoporous Quartz Superlattice. *Angew. Chem., Int. Ed.* **2016**, *55* (20), 6008−6012.
(44) Putz, F.; Scherer, S.; Ober, M.; Morak, R.; Paris, O.; Hüsing, N. 3D Printing of Hierarchical Porous Silica and α-Quartz. *Adv. Mater. Technol.* **2018**, *3* (7), 1800060.
(45) Zhang, Q.; Sánchez-Fuentes, D.; Gómez, A.; Desgarceaux, R.; Charlot, B.; Gàzquez, J.; Carretero-Genevrier, A.; Gich, M. Tailoring the Crystal Growth of Quartz on Silicon for Patterning Epitaxial Piezoelectric Films. *Nanoscale Adv.* **2019**, *1* (9), 3741−3752.
(46) Lin, C.-C.; Chen, S.-F.; Liu, L.; Li, C.-C. Size Effects of Modifying Cations on the Structure and Elastic Properties of Na2O−MO−SiO2 Glasses (M = Mg, Ca, Sr, Ba). *Mater. Chem. Phys.* **2010**, *123* (2), 569−580.
(47) Carretero-Genevrier, A.; Drisko, G. L.; Grosso, D.; Boissiere, C.; Sanchez, C. Mesoscopically Structured Nanocrystalline Metal Oxide Thin Films. *Nanoscale* **2014**, *6* (23), 14025−14043.
(48) Bertone, J. F.; Cizeron, J.; Wahi, R. K.; Bosworth, J. K.; Colvin, V. L. Hydrothermal Synthesis of Quartz Nanocrystals. *Nano Lett.* **2003**, *3* (5), 655−659.
(49) Zhang, Q.; Sánchez-Fuentes, D.; Desgarceaux, R.; Escofet-Majoral, P.; Oró-soler, J.; Gázquez, J.; Larrieu, G.; Charlot, B.; Gómez, A.; Gich, M.; Carretero-Genevrier, A. Micro/Nanostructure Engineering of Epitaxial Piezoelectric α-Quartz Thin Films on Silicon. *ACS Appl. Mater. Interfaces* **2020**, *12* (4), 4732−4740.
(50) Gomez, A.; Gich, M.; Carretero-Genevrier, A.; Puig, T.; Obradors, X. Piezo-Generated Charge Mapping Revealed through Direct Piezoelectric Force Microscopy. *Nat. Commun.* **2017**, *8* (1), 1113.
(51) Sohn, Y.-I.; Miller, R.; Venkataraman, V.; Lončar, M. Mechanical and Optical Nanodevices in Single-Crystal Quartz. *Appl. Phys. Lett.* **2017**, *111* (26), 263103.
(52) Jolly, C.; Sanchez-Fuentes, D.; Garcia-Bermejo, R.; Cakiroglu, D.; Carretero-Genevrier, A. Carretero-Genevrier, A. Epitaxial Nanostructured α-Quartz Films on Silicon: From the Material to New Devices. *J. Vis. Exp.* **2020**, No. 164, No. e61766.

https://doi.org/10.1021/acs.accounts.1c00592
Acc. Chem. Res. XXXX, XXX, XXX−XXX

(53) Jolly, C.; Gomez, A.; Sánchez-Fuentes, D.; Cakiroglu, D.; Rathar, R.; Maurin, N.; Garcia-Bermejo, R.; Charlot, B.; Gich, M.; Bahriz, M.; Picas, L.; Carretero-Genevrier, A. Soft-Chemistry-Assisted On-Chip Integration of Nanostructured α-Quartz Microelectromechanical System. *Adv. Mater. Technol.* **2021**, *6* (3), 2000831.
(54) Bye, G. C.; Simpkin, G. T. Influence of Cr and Fe on Formation of α-Al2O3 from γ-Al2O3. *J. Am. Ceram. Soc.* **1974**, *57* (8), 367−371.
(55) Xue, L. A.; Chen, I. Influence of Additives on the γ-to-α Transformation of Alumina. *J. Mater. Sci. Lett.* **1992**, *11* (8), 443−445.
(56) Okada, K.; Hattori, A.; Taniguchi, T.; Nukui, A.; Das, R. N. Effect of Divalent Cation Additives on the γ-Al2O3-to-α-Al2O3 Phase Transition. *J. Am. Ceram. Soc.* **2000**, *83* (4), 928−932.
(57) Wu, Y.; Zhang, Y.; Pezzotti, G.; Guo, J. Influence of AlF3 and ZnF2 on the Phase Transformation of Gamma to Alpha Alumina. *Mater. Lett.* **2002**, *52* (4), 366−369.
(58) Okada, K.; Hattori, A.; Kameshima, Y.; Yasumori, A. Concentration Effect of Cs+ Additive on the γ-Al2O3-to-α-Al2O3 Phase Transition. *Mater. Lett.* **2000**, *42* (3), 175−178.
(59) Okada, K.; Hattori, A.; Kameshima, Y.; Yasumori, A.; Das, R. N. Effect of Monovalent Cation Additives on the γ-Al2O3-to-α-Al2O3 Phase Transition. *J. Am. Ceram. Soc.* **2000**, *83* (5), 1233−1236.
(60) Živkovic, Ž.; Štrbac, N.; Šesták, J. Influence of Fluorides on Polymorphous Transformation of α-Al2O3 Formation. *Thermochim. Acta* **1995**, *266*, 293−300.
(61) Li, J.; Wu, Y.; Pan, Y.; Liu, W.; Guo, J. Influence of Fluorides on Phase Transition of α-Al2O3 Formation. *Ceram. Int.* **2007**, *33* (6), 919−923.
(62) Choi, J.-S.; Lee, S. W.; Kim, Y. H. Low-Temperature Synthesis of α-Alumina Using NaCl−Na3AlF6 Flux. *Ceram. Int.* **2020**, *46* (9), 13233−13239.
(63) Hwang, A. Y.; Kim, S. T.; Ji, H.; Shin, Y.; Jeong, J. K. Metal-Induced Crystallization of Amorphous Zinc Tin Oxide Semiconductors for High Mobility Thin-Film Transistors. *Appl. Phys. Lett.* **2016**, *108* (15), 152111.
(64) Shin, Y.; Kim, S. T.; Kim, K.; Kim, M. Y.; Oh, S.; Jeong, J. K. The Mobility Enhancement of Indium Gallium Zinc Oxide Transistors via Low-Temperature Crystallization Using a Tantalum Catalytic Layer. *Sci. Rep.* **2017**, *7* (1), 10885.
(65) Kim, T.; Kim, M. J.; Lee, J.; Jeong, J. K. Boosting Carrier Mobility in Zinc Oxynitride Thin-Film Transistors via Tantalum Oxide Encapsulation. *ACS Appl. Mater. Interfaces* **2019**, *11* (25), 22501−22509.
(66) Lee, S. H.; Lee, S.; Jang, S. C.; On, N.; Kim, H.-S.; Jeong, J. K. Mobility Enhancement of Indium-Gallium Oxide via Oxygen Diffusion Induced by a Metal Catalytic Layer. *J. Alloys Compd.* **2021**, *862*, 158009.
(67) Jeong, S.; Jang, S.; Han, H.; Kim, H.; Choi, C. C-Axis Aligned Crystalline Indium-Gallium-Zinc Oxide (CAAC-IGZO) and High-k Charge Trapping Film for Flash Memory Application. *J. Alloys Compd.* **2021**, *888*, 161440.
(68) Cho, G.; Joo, H.; Lee, H.; Nam, T.; Choi, H.; Huh, S.; Choi, B.; Jeong, H.; Noh, J. Microstructural and Electrochemical Properties of LiCoO2 Thin Films Prepared by Metal-Induced Crystallization. *J. Nanosci. Nanotechnol.* **2015**, *15* (10), 8187−8190.
(69) Cheyns, D.; Kam, B.; Vasseur, K.; Heremans, P.; Rand, B. P. Structure Induced Conductivity Enhancement in Metal-Doped Molybdenum Oxide Thin Films. *J. Appl. Phys.* **2013**, *113* (4), No. 043109.
(70) Karvinen, S. The Effects of Trace Elements on the Crystal Properties of TiO2. *Solid State Sci.* **2003**, *5* (5), 811−819.
(71) Brinker, C. J.; Clem, P. G. Quartz on Silicon. *Science* **2013**, *340* (6134), 818−819.

https://doi.org/10.1021/acs.accounts.1c00592
Acc. Chem. Res. XXXX, XXX, XXX−XXX